

## Organic Polymer Light-Emitting Devices on Flexible Plastic Substrates for AM-OPLED

*Yongtaek Hong and Jerzy Kanicki*

Organic & Molecular Electronics Laboratory, Solid State Electronics Laboratory,  
Dept. of Electrical Engineering and Computer Science, University of Michigan, Ann Arbor, MI 48109

### Abstract

The opto-electronic properties of the organic polymer light-emitting devices (OPLEDs) fabricated on flexible plastic substrates have been studied for active-matrix organic polymer light-emitting display (AM-OPLED) applications. The characterization was done for both green and red light OPLEDs. The hole injection layer and hole transport layer were used in OPLEDs for optimum opto-electronic device performances. The effect of different cathode-metalization methods, such as thermal and electron-beam evaporations, on the device performances has also been investigated.

### Introduction

Over last several years, there is a tremendous interest in the organic polymer light-emitting devices (OPLEDs) fabricated on flexible plastic substrates. Among different flat panel display (FPD) technologies, most likely OPLEDs are the most suitable for flexible plastic substrates. So far, only a few groups have reported small molecule-based OLEDs on flexible plastic substrates.<sup>1</sup> Our group has worked on OPLEDs on flexible plastic substrates over last several years.<sup>2,3</sup>

In this paper, we report the opto-electronic performances of the red and green light-emitting devices fabricated on flexible substrates for active-matrix organic polymer light emitting display (AM-OPLED) applications.

### Experimental

Figure 1 shows the schematic of the measurement system used in this study. The integrating sphere was used to collect all the light emission from the devices. The electrical and optical data acquisitions were controlled by a personal computer. The electroluminescence (EL) was measured with a calibrated CCD spectrum system.

The plastic substrates with patterned ITO electrodes, which have the sheet resistance of about 12.2 ohms/square and the transmission greater than 80 % over the visible range were used. The substrate size is 2"×2". The substrates were cleaned in the ultrasonic bath of isopropanol. Without any ITO surface treatment, hole injection layer (HIL), hole transport layer (HTL) and light emissive layer (LEL) were sequentially spin coated and cured in the vacuum oven. Then, aluminum cathode was

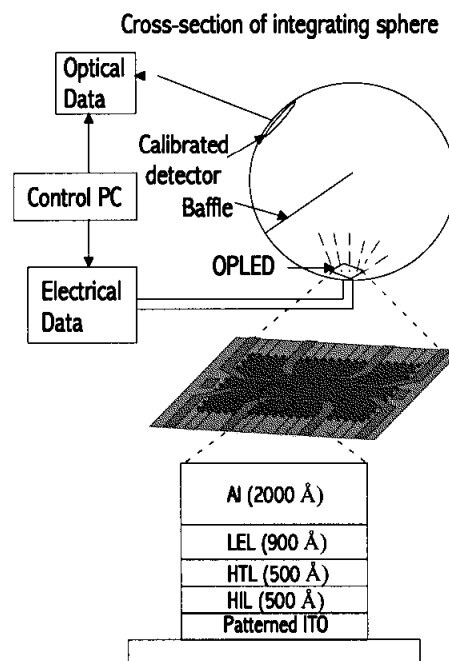
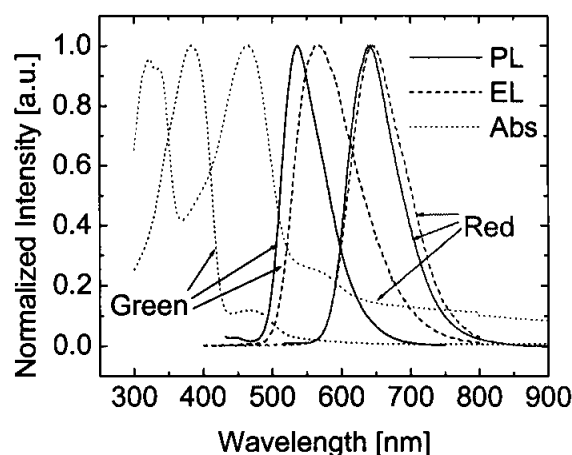


Figure 1 Device structure and measurement setup used in this work.

thermally or electron-beam evaporated through shadow masks under a high vacuum condition ( $\sim 10^{-6}$  Torr). The device area defined by the cross-section of anode and cathode is  $0.05'' \times 0.05''$ .

### Results and Discussions

As shown in Fig. 1, multi-layer structures were used to improve OPLEDs opto-electronic performances. The PEDOT/PSS, PC6, and Dow red



(a)

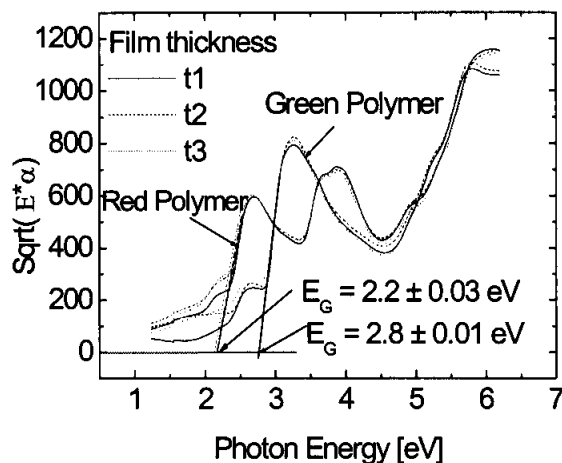
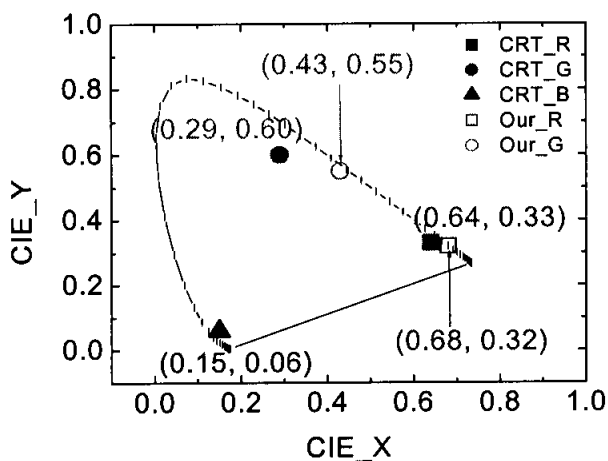


Figure 2. Photoluminescence, electroluminescence, and absorption spectra (a), and CIE data (b) of the green and red light emitting polymers are shown.

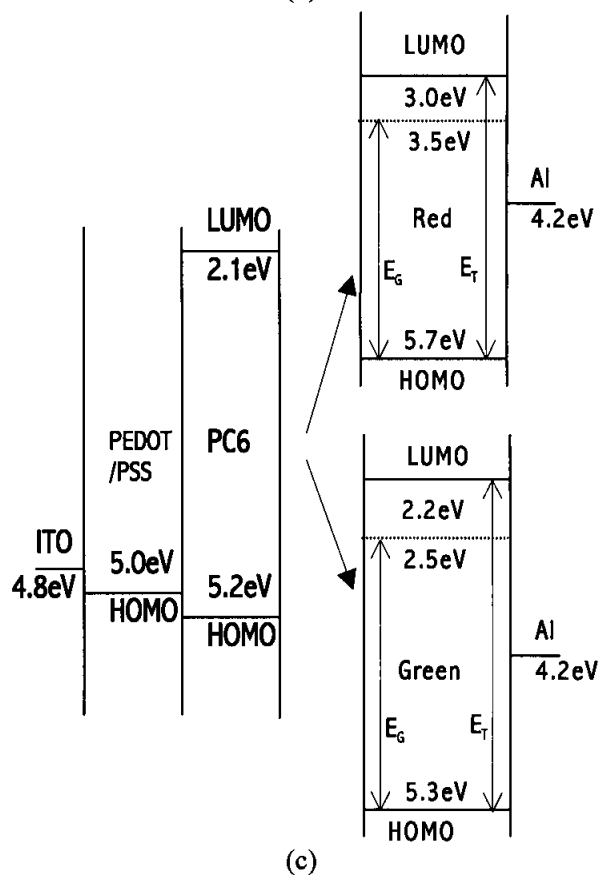
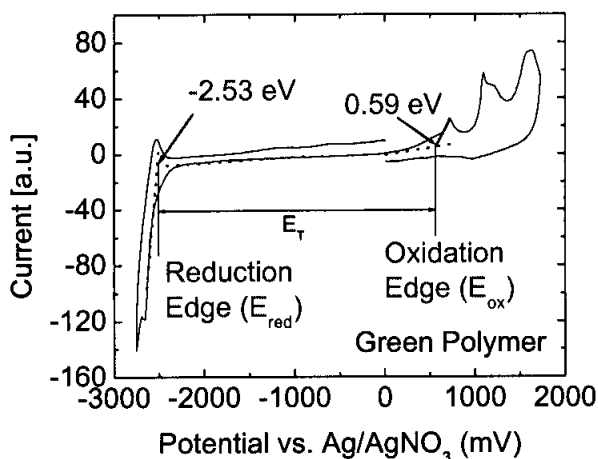
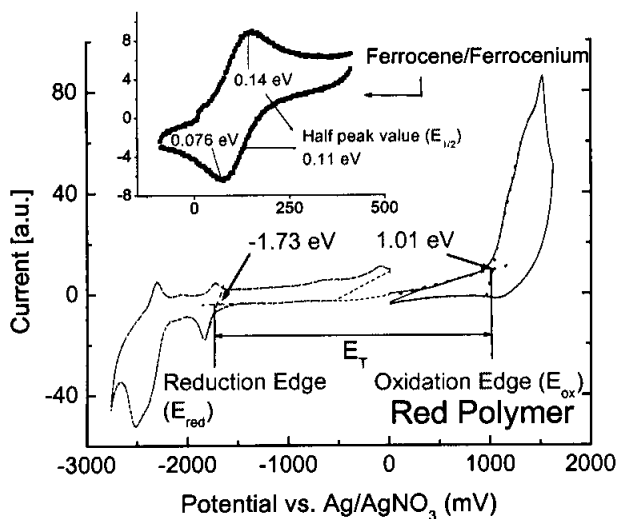


Figure 3 Cyclic voltammety data (a) and Tauc plots (b) for light emissive polymers are shown; t1, t2, and t3 represent 1000/2000, 800/1000, 600/700 Å for red/green polymers, respectively. Energy band diagram (c) extracted from (a) and (b);  $E_T$  and  $E_G$  are transport and optical band gaps, respectively.

/green light-emitting polymers were used for HIL, HTL, LEL, respectively. The material characteristics of the PEDOT/PSS and PC6 have been reported elsewhere.<sup>4,5</sup> Fig. 2(a) shows the photoluminescence (PL), electroluminescence (EL), and absorption (Abs) spectra of the Dow green and red light emitting polymers. The absorption and PL spectra were

obtained for several single layer thin films deposited on quartz substrates with different thickness. The EL spectra were measured for ITO/HIL/LEL/aluminum structure. The peak values of Abs/PL/EL for green and red LEL are 383/537/568-nm and 465/639/644-nm, respectively. The EL spectra of both the green and red light-emitting polymers are red-shifted with respect to PL. From EL spectra, Commission Internationale de l'Eclairage (CIE) data for our two light-emitting polymers have been obtained as shown in Fig. 2(b). The CIE values for cathode ray tube (CRT) red, green, and blue light emission are also given in this figure. We obtained (0.43, 0.55) and (0.68, 0.32) for Dow green and red light-emitting polymers, respectively. From the figure, it is found that our polymers can be used for full color AM-OLED applications once the blue light-emitting polymer is added.

To develop the energy band diagram of our devices, we used a combination of the cyclic voltammetry (CV) and Tauc plots of the absorption spectra. From the CV spectra shown in Fig. 3(a), the positions of the lowest unoccupied molecular orbital (LUMO) and highest occupied molecular orbital (HOMO) with respect to the vacuum energy level, and the transport band gap ( $E_T$ ) have been obtained by using the following procedures. The onsets of oxidation ( $E_{ox}$ ) and reduction ( $E_{red}$ ) are obtained from the measured CV spectra. In our case, we observed two reduction and oxidation peaks for red and green LEL, respectively. However, since we believe that the first reduction and oxidation potentials represent the triggering point of reduction and oxidation processes, we used these values to define LUMO and HOMO levels for our light emissive polymers. By assuming a scale factor relating Ferrocene/Ferrocenium couple to vacuum of  $\sim 4.8$  eV<sup>4</sup>, the HOMO and LUMO levels can be defined by measuring  $E_{ox}$ ,  $E_{red}$ , and  $E_{1/2}$ .

$$\text{HOMO} = (E_{ox} - E_{1/2}) + 4.8 \text{ [eV]},$$

$$\text{LUMO} = (E_{red} - E_{1/2}) + 4.8 \text{ [eV]},$$

where,  $E_{1/2}$  is the averaged half peak value of ferrocene level. In our case, HOMO and LUMO levels of red/green light-emitting polymers are 5.7/5.7 eV and 3.0/2.6 eV, respectively.

The polymer optical band gap energy ( $E_G$ ) was obtained from the Tauc plot of absorption spectra shown in Fig 3(b). If we assume that our spin-coated polymers are amorphous 3-D system, in which the electron wave functions can spread in all directions, the following equation can be derived.<sup>6</sup>

$$\sqrt{\alpha \hbar \omega} \propto (\hbar \omega - E_G)$$

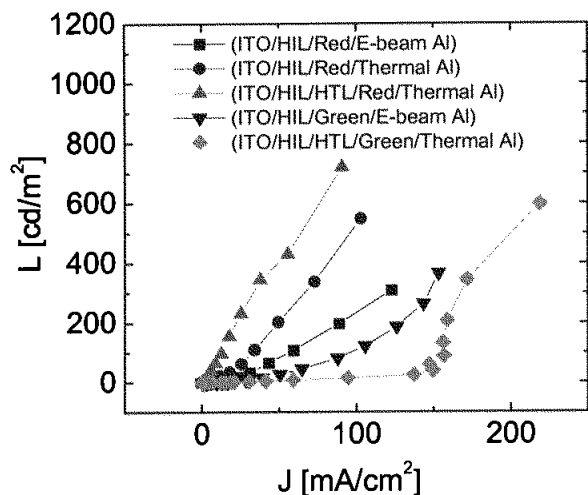
where  $\alpha$  and  $\hbar \omega$  are absorption coefficient and photon energy, respectively. This equation shows that optical band gap can be extrapolated when the square

root of the product of absorption coefficient and photon energy is plotted versus photon energy. In Fig. 3(b), Tauc plots and linear fits for our emissive polymers with different thickness are shown. From this figure, we extracted  $E_G = 2.2 \pm 0.03$  eV and  $2.8 \pm 0.01$  eV for red and green polymers, respectively. Using the above extracted energy level values, the energy band diagram for our double layer OLEDs was constructed as shown in Fig. 3 (c). The HOMO level of PEDOT/PSS and work functions of Al and ITO are also included. By combining HIL and HTL in one OLED structure, the effective hole injection barrier is reduced from 0.9/0.5 eV to three steps of 0.2/0.2, 0.2/0.2, and 0.7/0.1 eV for red/green light-emitting polymers, respectively. For red devices, this staircase-like gradual increase of the HOMO levels between ITO and LEL enhances the device brightness and efficiencies measured at the same current densities as shown in Fig. 4, where emission (EE) and power (PE) efficiencies are defined by the ratio of brightness to current flow across the devices and the ratio of light output power to electrical input power, respectively. These improvements are due to reduction of effective barrier for hole injection into LEL.

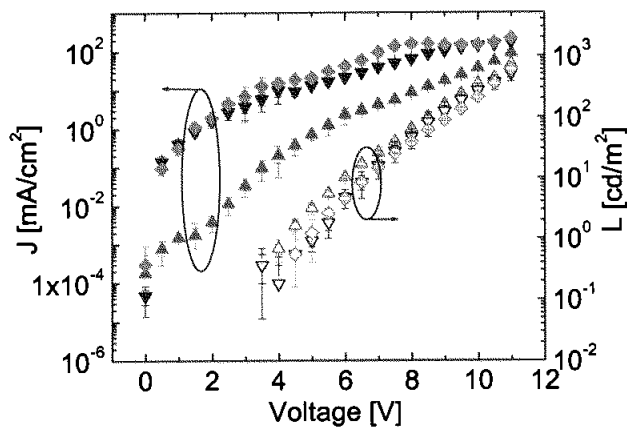
For green OLEDs, slightly poorer device performances have been obtained in comparison with the red OLEDs. The same device structures, e.g. ITO/HIL/LEL/e-beam Al and ITO/HIL/HTL/LEL/thermal Al were used in both cases. We speculate that this difference is due to larger electron injection barrier at the cathode of the green devices (about 0.8 – 1.0 eV larger than barrier of the red devices). From Fig. 4(a), the L-J characteristics of green devices do not show the linear relationship over the whole current levels in comparison with the red devices. This behavior is more apparent for the devices with the HIL (two linear segments). Also the total current flow increased for green OLED with HIL in comparison with the devices without HIL while the light output did not change that much for the same voltage levels as shown in Fig. 4(b). This observation can indicate that the holes contribution to the total current flow is larger when HIL is added in the device structure. This additional layer will reduce effective hole injection barrier between anode and LEL. At the same time in this structure, however, a higher electron injection barrier limits the optical device performances by reducing the electron density at the LEL/cathode interface. From our results, we can conclude that the electron injection barrier at the cathode is the limiting factor in the green OLED performance optimization. Therefore, green device opto-

electronic performances can only be improved if a low work function metal cathode, such as calcium or erbium is used, and/or an additional electron injection layer between LEL and cathode is introduced. These issues will be discussed in a separate publication.

We have also investigated the effect of different cathode-metalization methods, such as electron-beam and thermal evaporation, on the optical and electrical performances of the OLEDs. From our results, we have concluded that devices with thermally evaporated cathodes have better opto-electronic performances. We speculate that this difference is associated either with the damage of LEL or metal migration to the inside of polymer induced by electron beam evaporation method. Both can cause deep gap states (defects) formation in the polymer and subsequent decrease in device luminance. The defects will trap electrons and reduce carrier recombination efficiency. It should be noticed that metal deposited by both methods has the same work function.



(a)



(b)

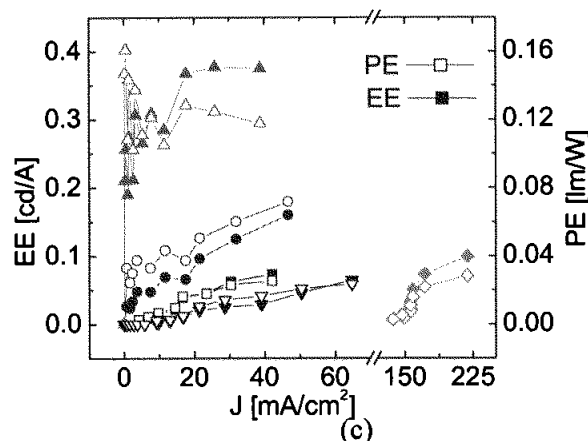


Figure 4 Optical and electrical performances of the red and green light-emitting devices fabricated on the flexible plastic substrates are shown, where PE and EE are power and emission efficiencies defined in the text, respectively.

### Conclusions

We have fabricated the multi-layer red and green OLEDs based on poly-fluorenes using aluminum as a cathode metal. We found that device optical and electrical performances can be improved by introducing a combination of the HIL and HTL in the device structure and by using a thermal evaporation method for cathode metal deposition. The following opto-electrical properties have been obtained for our red/green OLEDs, respectively: turn-on voltage:  $\sim 3.5/5.0$  V; voltage and current density at  $100 \text{ cd/m}^2$ :  $\sim 8/9.1$  V and  $\sim 15/150 \text{ mA/cm}^2$ ; maximum light emission and power efficiencies at  $\sim 20/220 \text{ mA/cm}^2$ :  $\sim 0.4/0.1 \text{ cd/A}$  and  $\sim 0.13/0.03 \text{ lm/W}$ .

### Acknowledgement

This research was supported by ONR-DARPA and NIH grants. Authors also thank Shujen Lee for PL and CV measurements.

### References

- 1 P.E. Burrows, G.L. Graff, M.E. Gross P.M. Martin, M. Hall, E. Mast, C. Bonham, W. Bennett, L. Michalski, M. Weaver, J.J. Brown, D. Fogarty, and L.S. Sapochak, *Proceedings of SPIE* **4105**, 75 (2001).
- 2 Y. He and J. Kanicki, *Proceedings of SPIE* **4105**, 143 (2001).
- 3 Y. Hong, Z. Hong, and J. Kanicki, *Proceedings of SPIE* **4105**, 356 (2001).
- 4 Y. Hong, Z. Hong, M.D. Curtis, and J. Kanicki, *Conference Record of the IDRC 2000*, 183 (2000)
- 5 Y. Hong, Z. He, S. Lee, and J. Kanicki, *Proceedings of SPIE* (in press).
- 6 J. Tauc, R. Grigorovici, and A. Vancu, *Phys. Stat. Sol.* **15**, 627 (1966).